International Journal of Fatigue 59 (2014) 9–13

Contents lists available at ScienceDirect

International Journal of Fatigue

journal homepage: www.elsevier.com/locate/ijfatigue

Technical note

Non-uniform deformation in a friction stir welded Mg–Al–Zn joint during stress fatigue

J. Yang, D.R. Ni, B.L. Xiao, Z.Y. Ma *

Shenyang National Laboratory for Materials Science, Institute of Metal Research, Chinese Academy of Sciences, 72 Wenhua Road, Shenyang 110016, China

ARTICLE INFO

Article history:
Received 12 June 2013
Received in revised form 25 September 2013
Accepted 9 October 2013
Available online 17 October 2013

Keywords:
Magnesium alloys
Friction stir welding
Stress fatigue
Texture

ABSTRACT

A friction stir welded (FSW) Mg–3Al–1Zn (AZ31) joint, prepared at a welding speed of 100 mm/min and a rotation rate of 800 rpm, was subjected to stress fatigue test. During fatigue deformation, while the specimen thickness shrank around the nugget zone (NZ)/thermomechanically-affected zone (TMAZ) boundary, it varied little in the NZ middle. Besides, the surface appearance differed between the two sides of a fatigued specimen. This non-uniform deformation was attributed to different grain orientation distributions and sheared material layers in various regions, which influenced the fatigue life and fracture behavior of the joint.

1. Introduction

Mg alloys are attractive in the aerospace and automotive industries due to their weight reduction and energy saving qualities. Some defects, such as porosity, oxidization, wide heat-affected zone, and high residual stress, are often produced in conventional fusion welded joints and these limit the use of Mg alloys. Friction stir welding (FSW), a solid joining method [1], is proved to be an enabling welding technique for joining Mg alloys [2,3].

The fatigue behavior of FSW joints of Mg alloys is an important consideration for the engineering design, and several investigations have been done recently. Most studies were focused on the analysis of fatigue data, including S–N curves [4–6], fracture surface examination [4,7], and fatigue crack growth behavior [7]. Padmanaban et al. [4,7] reported that the fatigue resistance of a FSW AZ31 joint was higher than that of the pulsed current gas tungsten arc welded joint. Chowdhury et al. [5] found that the fatigue strength of a FSW AZ31 joint was affected by the pin thread orientation. However, to the authors' knowledge, no work on the fatigue deformation mechanism of FSW joints of Mg alloys is reported in the open literature so far, though similar work was reported for wrought Mg alloy [8–10].

In the wrought Mg alloys, the strong basal texture has a significant effect on the fatigue deformation behavior [8,9]. Unlike the wrought alloys, the nugget zones of FSW joints have a unique texture distribution with the basal plane roughly rotated around the pin surface in the NZ [11]. This causes some difficulties in the analysis of the deformation mechanism during both uniaxial tension and fatigue tests. The deformation mechanism of FSW AZ31 joints during uniaxial tension has recently been investigated by Xin et al. [12] and Yang et al. [13]. It was revealed that the region around the NZ/TMAZ boundary was prone to neck and the NZ middle suffered from the least deformation during tension, which was attributed to the texture distribution. The fatigue deformation of FSW Mg joints should definitely be affected by the heterogeneous microstructure, but the correlative work is lacking.

In this study, the FSW joint of a rolled AZ31 Mg alloy plate was subjected to stress fatigue investigation. The aim is to understand the effect of the texture distribution on the fatigue properties and deformation behavior of the FSW AZ31 joint.

2. Materials and experiments

6.4 mm thick AZ31-H24 plate was used in this study. FSW tool with a shoulder 24 mm in diameter and a cylindrical threaded pin 8 mm in diameter and 5.9 mm in length was used. FSW was conducted along the rolling direction (RD) at a welding speed of 100 mm/min and a rotation rate of 800 rpm, with a tool tilt angle of 2.8°. The schematic of the FSW process is shown in Fig. 1a. The advancing side, where the traveling and rotating directions of the tool are the same, and the retreating side, where the traveling and rotating directions of the tool are the opposite, is written as the AS and RS, respectively, throughout this paper. Three directions of the rolled plate were named as the normal direction (ND), the transverse direction (TD), and the RD, respectively, as shown in Fig. 1a.

* Corresponding author. Tel./fax: +86 24 83978908.
E-mail address: zyma@imr.ac.cn (Z.Y. Ma).

0142-1123/$ - see front matter © 2013 Elsevier Ltd. All rights reserved.
http://dx.doi.org/10.1016/j.ijfatigue.2013.10.004

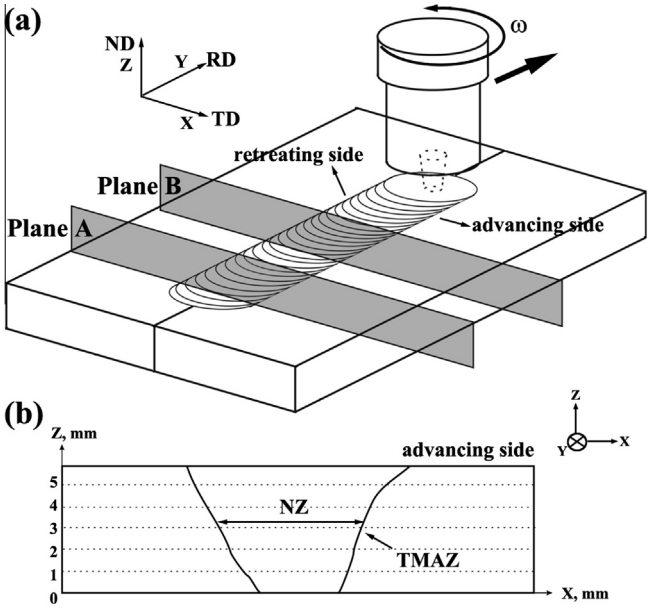

Fig. 1. Schematic of (a) FSW process and (b) positions of contour profile measurement for specimen after fatigue deformation.

The specimens for microstructure examinations were cut perpendicular to the welding direction (i.e. RD). Microstructure characterization and analysis were carried out by optical microscopy (OM), scanning electron microscopy (SEM, Hitachi S-3400N) and electron backscattered diffraction (EBSD, HKL). Transverse tensile specimens with a gauge length of 40 mm and a gage width of 10 mm were machined, and tested at a strain rate of 1×10^{-3} s^{-1} on a Zwick/Roell Z050 tester. The results of tensile tests were taken from three or four specimens.

Fatigue specimens referring to ASTM E466 standard, with a parallel section of $50 \times 13 \times 5.8$ mm in size, were machined perpendicular to the welding direction. The fatigue specimens were ground with SiC papers up to grit 2000 to remove the machining marks and to achieve a consistent and smooth surface. Fatigue tests were performed on an MTS fatigue tester at $R = 0$ in air at room temperature, with a frequency of 30 Hz. Plane A and plane B are the two sides of a specimen, where the tool passed plane A earlier than plane B during the FSW process. After fatigue deformation, the contour profile was measured on plane A and plane B of the fatigue specimen using an Alpha-Step IQ surface profiler. At Z values (thickness) of 1, 2, 3, 4 and 5 mm, the relationship between X (distance)-Y (height) was measured, as schematically shown in Fig. 1b. During measurement, the Y value of the parent material (PM) is used as a reference, which is set as zero.

3. Results and discussion

3.1. Fatigue life

Fig. 2 shows the S–N curve of the PM and the FSW joint. When the stress amplitude was only 5 MPa higher than the fatigue strength, the fatigue life of the PM was decreased to about 7.2×10^4 cycles. Similar result was also observed in the FSW AZ31 joint. This phenomenon was also reported in other studies of wrought AZ31 alloy [14,15], and the reason was attributed to the different modes of crack initiation and propagation at stress amplitudes near and slightly higher than the fatigue strength. At stress amplitudes higher than the fatigue strength, a large number of cracks developed and they were easy to propagate across the grain boundaries; but at stress amplitudes near the fatigue

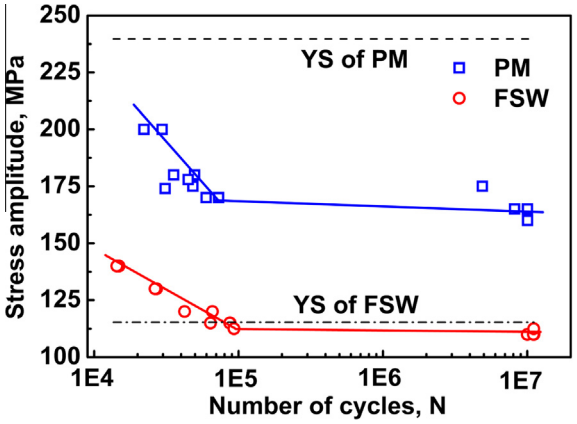

Fig. 2. S–N curves of FSW AZ31 joints and parent material.

strength, there were few cracks, which were not easy to propagate [14,15].

On the S–N curve, the PM exhibited a fatigue strength of 160 MPa, 80 MPa lower than the yield strength (YS), which is consistent with the fatigue results of wrought AZ31 and AZ61 alloys [6,16,17]. However, compared with the PM, the joint exhibited a fatigue strength of 110 MPa similar to the YS (115 MPa); the specific reason will be discussed below.

3.2. Fatigue deformation and failure

In the cross sections of the FSW joints of Mg alloys, three microstructural zones could be identified: NZ, TMAZ, and heat-affected zone (HAZ) and the position of NZ and TMAZ are shown in Fig. 1b. Fig. 3a shows the macro-image of the joints that experienced fatigue deformation. Non-uniform deformation was observed for the specimens at all stress amplitudes. It is noted that after the fatigue test, plane B exhibited a more severe deformation appearance with a macroscopic bulge in the NZ, and this bulge was more obvious at the high amplitudes. However, no such bulge was observed on plane A. Furthermore, at the high stress amplitudes, the specimen failed along the NZ/TMAZ boundary on the AS.

The contour profile was measured for the joint at a strain amplitude of 110 MPa (Fig. 3b). On plane A, the whole NZ surface was about 50 μm lower than the PM surface; on plane B, the NZ middle protruded and the two sides sank, with the protuberant part 90 μm higher than the PM surface and the sunken part 50 μm lower. For the whole joint, the thickness reduction occurred around the NZ/TMAZ boundary on both the AS and RS during the fatigue deformation, and these regions shrank; with the thickness of the PM as a reference, the NZ middle had little variation about the thickness, but projected towards plane B. Besides, it could be found that the fracture path of specimens was consistent with the thickness reduction around the NZ/TMAZ boundary on the AS.

Therefore, the non-uniform deformation was produced not only in different regions of the joint, but also on different sides of a single specimen, which was characterized by the thickness variation of the joints and the different appearances between plane A and plane B, respectively. In Fig. 3b, it is noted that this non-uniform deformation could be detected even at the stress amplitude near fatigue strength, and the increase in stress amplitude only increased the degree of the deformation. Therefore, the cause of the non-uniform deformation could be focused on the specimens near the fatigue strength.

Because the PM had a relatively uniform structure with a strong rolling macro texture, the deformation ability varied little in the PM and thus no obvious fluctuation was observed on the surface. However, the FSW AZ31 joints had non-uniform microstructures

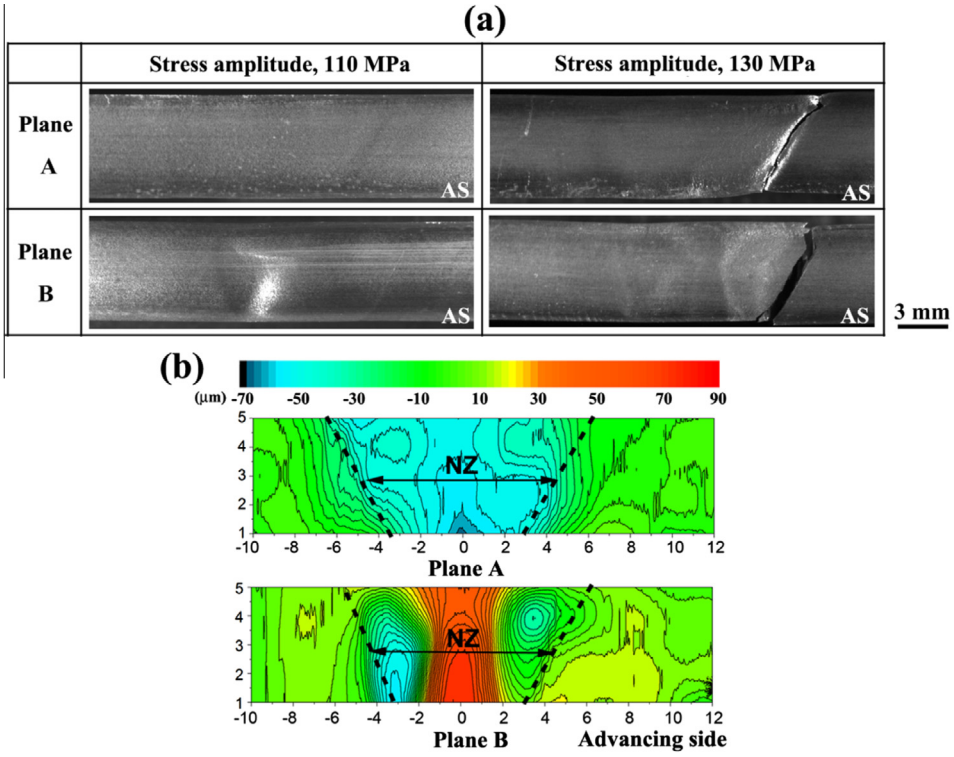

Fig. 3. (a) Macro image of FSW AZ31 joints at different stress amplitudes; and (b) contour profile of the cross section at a stress amplitude of 110 MPa.

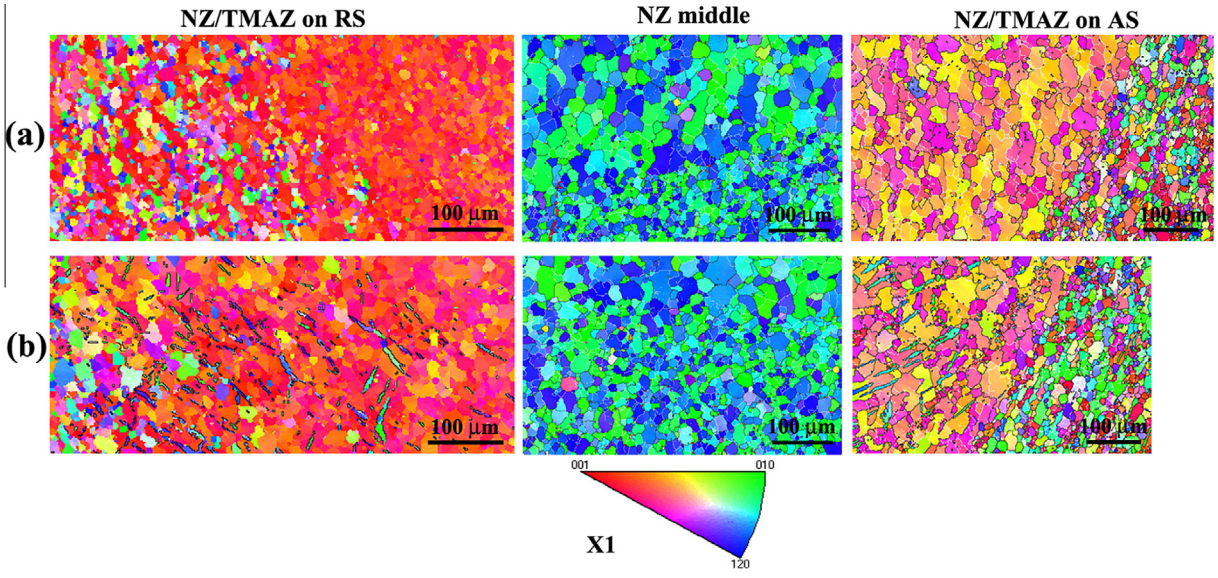

Fig. 4. EBSD inverse pole figure maps at different regions of FSW AZ31 joint for (a) specimen before fatigue deformation and (b) fatigue specimen at a stress amplitude of 110 MPa.

[11], as displayed by the inhomogeneous distribution of grain orientation (Fig. 4a). The Schmid factor (SF) for basal slip at different regions is shown in Table 1. The NZ middle with an equiaxed grain structure exhibited little orientation variation with a mean SF of about 0.1. On the NZ/TMAZ boundary, the grain orientation had an obvious difference between the NZ side and the TMAZ side: the grains in the NZ side had a similar orientation with a mean SF of about 0.45, while the grain orientation in the TMAZ side was more dispersive with a mean SF of about 0.35. Similar results were also found in our previous study [13]. This could be attributed to the different deformation degrees between the two sides of the NZ/TMAZ boundary during FSW: the NZ experienced severe plastic deformation, while the TMAZ suffered from less plastic deformation. Besides, it is noted that this difference was more distinct on the AS than on the RS, due to different material flow patterns. During FSW, the material on the AS is rotated by the stir pin, and then deposits on the RS, resulting in more serious deformation on the AS [18].

After the fatigue deformation, the grain orientation had different variations in the different regions (Fig. 4b). In the NZ middle, little variation was found for the following reasons. First, the basal slip could not be activated for the low SF. Second, the *c* axis was

Table 1
Schmid factor for basal slip at different regions of FSW AZ31 joint.

	NZ middle	NZ/TMAZ boundary on AS		NZ/TMAZ boundary on RS	
		NZ side	TMAZ side	NZ side	TMAZ side
Range	0–0.2	0.4–0.5	0.15–0.5	0.4–0.5	0.3–0.5
Mean value	0.1	0.45	0.35	0.45	0.4

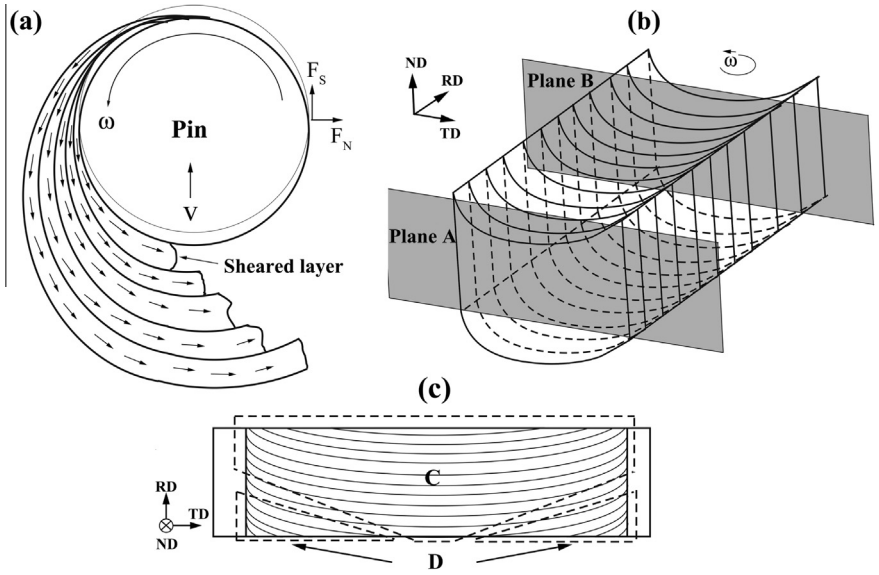

Fig. 5. Schematic illustration of sheared layers in FSW joint: (a) formation of sheared layer [24], distribution of sheared layers viewed in (b) rolling direction and (c) normal direction.

perpendicular to the load direction with tensile twinning being suppressed. Third, at the stress amplitude near YS, compression twinning could not develop. In other words, because of the grain orientation against deformation, the NZ middle had the hard orientation (The grain orientations favorable for basal slip are defined as 'soft orientations', otherwise defined as 'hard orientations') [19], thus the thickness of the NZ middle showed little variation during fatigue deformation.

However, while some tensile twins were detected on the NZ/TMAZ boundary at the NZ side, few twins were observed in the adjacent NZ (Fig. 4b). This could be attributed to the different deformation abilities. The NZ side was prone to basal slip at lower stress amplitude for a high SF of about 0.4–0.5. However, the TMAZ side was more difficult to deform due to the dispersive grain orientation and the lower mean SF. Because of the incompatible deformation between the TMAZ and NZ sides, tensile twinning was activated in order to coordinate plastic deformation. According to a former study [20], this tensile twinning could also produce some strain. Therefore, under the influence of both the basal slip and twinning, large plastic deformation occurred around the NZ/TMAZ boundary with obvious thickness shrinkage (Fig. 3b).

Based on Fig. 3, two kinds of non-uniform deformations were observed during the fatigue deformation. The first one, characterized by the variation in the thickness of the joint, could be related to the different deformation abilities in the various regions, as per the analyses above. This kind of non-uniform deformation could influence the fatigue strength and fracture behavior. For a high SF, when the applied stress reached the global YS of the joint, the grains around the NZ/TMAZ boundary could be under a stress exceeding the YS point, and thus tensile twinning occurred in this region [13]. Similarly, during tensile stress-controlled fatigue, when the stress amplitude was close to the YS, the plastic deformation developed partly around the NZ/TMAZ boundary with some tensile twins appearing (Fig. 4b). Although twin accumulation could induce material fracture [21,22], at the stress amplitude near the YS, the twin fraction was small and the deformation degree was low in the joint, which might not lead to fracture. Therefore, the fatigue strength of the joint was close to the YS (Fig. 2). When the stress amplitude was higher than the YS, the degree of deformation increased and more tensile twins were activated on the NZ/TMAZ boundary, which has been proved by the twinning evolution during the tension [13]. Besides, the variation of grain orientation between the NZ and TMAZ sides was more significant on the AS than on the RS, so that the incompatible deformation on the NZ/TMAZ boundary was more serious on the AS. As a result, the fatigue specimens fractured along the NZ/TMAZ boundary on the AS (Fig. 3a).

The second kind of non-uniform deformation, characterized by different surface appearances between plane A and plane B (Fig. 3a and b), was only observed in the FSW specimens. Because some factors, such as distribution of the grain size and texture, did not differ between the two planes of a single specimen, this phenomenon could be related to a factor caused by the FSW process.

3.3. Mode of non-uniform deformation

By the shear effect of the stir pin, the material was rotated round the pin surface during FSW. Krishnan [23] suggested that the hot metal was extruded within each revolution. Furthermore, using the pin-breaking technique, Chen et al. [24,25] revealed that the sheared material around the pin was spread into a layer at each revolution; as the FSW proceeded, more layers could be formed [24]. According to their study [24], these processes could be shown by the schematic drawings in Fig. 5a.

After the plates were welded, these sheared material layers were consecutively distributed in the joint (Fig. 5b). However,

when the fatigue specimens were cut from the joint, the distribution of sheared layers differed between plane A and plane B (Fig. 5c). On plane B, these layers were almost integrated with only a length reduction. However, on plane A, most layers were cut into two parts and located on the two sides of the NZ, while the integrated layers were only observed in the NZ middle. The integrated layers and broken layers were marked by regions C and D, respectively (Fig. 5c). It is clear that region C was much larger than region D on plane A.

During fatigue deformation, a tensile stress was applied on the specimen along the transverse direction (TD). Deformation of the integrated layers was more difficult than that of the broken ones. Therefore, the material in region D could deform more easily than that in region C in the joint. Because plane B contained continuous layers (region C), different layers had a similar deformation ability. Thus, the surface fluctuation after fatigue deformation resulted from the texture distribution, as discussed above. However, on plane A, region D was much larger than region C, and thus the surface sinking of the whole NZ was caused by the movement of region D.

4. Conclusions

In summary, for the FSW AZ31 joint, the grains had a hard orientation in the NZ middle and a soft orientation around the NZ/TMAZ boundary, resulting in invariant thickness in the NZ middle and a thickness shrinkage around the NZ/TMAZ boundary during fatigue deformation. For this non-uniform deformation, the fatigue strength of the FSW joints was close to the yield strength, with failure along the NZ/TMAZ boundary on the AS at higher stress amplitudes. Moreover, because the distribution of sheared layers differed between the two sides of a fatigue specimen, the NZ middle projected to one side after fatigue testing.

Acknowledgements

This work was supported by the National R&D Program of China under Grant No. 2011BAE22B05 and the National Natural Science Foundation of China under Grant Nos. 51371179 and 51331008.

References

[1] Mishra RS, Ma ZY. Friction stir welding and processing. Mater Sci Eng R 2005;50:1–78.
[2] Yang J, Xiao BL, Wang D, Ma ZY. Effects of heat input on tensile properties and fracture behavior of friction stir welded Mg–3Al–1Zn alloy. Mater Sci Eng A 2010;527:708–14.
[3] Commin L, Dumont M, Masse JE, Barrallier L. Friction stir welding of AZ31 magnesium alloy rolled sheets: influence of processing parameters. Acta Mater 2009;57:326–34.
[4] Padmanaban G, Balasubramanian V. Fatigue performance of pulsed current gas tungsten arc, friction stir and laser beam welded AZ31B magnesium alloy joints. Mater Des 2010;31:3724–32.
[5] Chowdhury SM, Chen DL, Bhole SD, Cao X. Effect of pin tool thread orientation on fatigue strength of friction stir welded AZ31B-H24 Mg butt joints. Procedia Eng, Fatigue 2010;2:825–33.
[6] Tsujikawa M, Somekawa H, Higashi K, Iwaskai H, Hasegawa T, Mizuta A. Fatigue of welded magnesium alloy joints. Mater Trans 2004;45:419–22.
[7] Padmanaban G, Balasubramanian V, Reddy GM. Fatigue crack growth behaviour of pulsed current gas tungsten arc, friction stir and laser beam welded AZ31B magnesium alloy joints. J Mater Process Technol 2011;211:1224–33.
[8] Yin SM, Yang F, Yang XM, Wu SD, Li SX, Li GY. The role of twinning-detwinning on fatigue fracture morphology of Mg–3%Al–1%Zn alloy. Mater Sci Eng A 2008;494:397–400.
[9] Park SH, Hong SG, Bang W, Lee CS. Effect of anisotropy on the low-cycle fatigue behavior of rolled AZ31 magnesium alloy. Mater Sci Eng A 2010;527:417–23.
[10] Wu L, Jain A, Brown DW, Stoica GM, Agnew SR, Clausen B, et al. Twinning-detwinning behavior during the strain-controlled low-cycle fatigue testing of a wrought magnesium alloy, ZK60A. Acta Mater 2008;56:688–95.
[11] Park SHC, Sato YS, Kokawa H. Basal plane texture and flow pattern in friction stir weld of a magnesium alloy. Metall Mater Trans A 2003;34A:987–94.
[12] Xin RL, Li B, Liao AL, Zhou Z, Liu Q. Correlation between texture variation and transverse tensile behavior of friction-stir-processed AZ31 Mg alloy. Metall Mater Trans A 2012;43A:2500–8.
[13] Yang J, Xiao BL, Wang D, Ma ZY. Effects of rotation rates on microstructure, mechanical properties, and fracture behavior of friction stir-welded (FSW) AZ31 magnesium alloy. Metall Mater Trans A 2013;44A:517–30.
[14] Nan ZY, Ishihara S, Goshima T, Nakanishi R. Scanning probe microscope observations of fatigue process in magnesium alloy AZ31 near the fatigue limit. Scr Mater 2004;50:429–34.
[15] Ishihara S, Nan Z, Goshirna T. Effect of microstructure on fatigue behavior of AZ31 magnesium alloy. Mater Sci Eng A 2007;468:214–22.
[16] Ogarevic VV, Stephens RI. Fatigue of magnesium alloys. In: Huggins RA, Giordmaine JA, Wachtman JB, editors. Annual review of mater sci, vol. 20. Palo Alto: Annual Reviews; 1990. p. 141–77.
[17] Tokaji K, Kamakura M, Ishiizumi Y, Hasegawa N. Fatigue behaviour and fracture mechanism of a rolled AZ31 magnesium alloy. Int J Fatigue 2004;26:1217–24.
[18] Xu S, Deng X. A study of texture patterns in friction stir welds. Acta Mater 2008;56:1326–41.
[19] Samman TA, Li X, Chowdhury SG. Orientation dependent slip and twinning during compression and tension of strongly textured magnesium AZ31 alloy. Mater Sci Eng A 2010;527:3450–63.
[20] Jiang L, Jonas JJ, Mishra RK, Luo AA, Sachdev AK, Godet S. Twinning and texture development in two Mg alloys subjected to loading along three different strain paths. Acta Mater 2007;55:3899–910.
[21] Koike J. Enhanced deformation mechanisms by anisotropic plasticity in polycrystalline Mg alloys at room temperature. Metall Mater Trans A 2005;36A:1689–96.
[22] Yang F, Yin SM, Li SX, Zhang ZF. Crack initiation mechanism of extruded AZ31 magnesium alloy in the very high cycle fatigue regime. Mater Sci Eng A 2008;491:131–6.
[23] Krishnan KN. On the formation of onion rings in friction stir welds. Mater Sci Eng A 2002;327:246–51.
[24] Chen ZW, Cui S. On the forming mechanism of banded structures in aluminium alloy friction stir welds. Scr Mater 2008;58:417–20.
[25] Chen ZW, Pasang T, Qi Y. Shear flow and formation of nugget zone during friction stir welding of aluminium alloy 5083-O. Mater Sci Eng A 2008;474:312–6.